

Quantitative Analysis of Dynamic Contrast-Enhanced and Diffusion-Weighted Magnetic Resonance Imaging for Oncology in R

Brandon Whitcher
Mango Solutions

Volker J. Schmid
Ludwig-Maximilians Universität München

Abstract

The package **dcemriS4** provides a complete set of data analysis tools for the quantitative assessment of dynamic contrast-enhanced MRI. Image processing is provided for the ANALYZE and NIFTI data formats as inputs with all parameter estimates being output in NIFTI format. Estimation of T1 relaxation from multiple flip-angle acquisitions, using either constant or spatially-varying flip angles, is performed via nonlinear regression. Both literature-based and data-driven arterial input functions are available and may be combined with a variety of compartmental models. Kinetic parameters are obtained from nonlinear regression, Bayesian estimation via Markov Chain Monte Carlo or Bayesian *maximum a posteriori* estimation. A non-parametric model, using penalized splines, is also available to characterize the contrast agent concentration time curves. Methods for quantification of diffusion-weighted MRI acquisitions common in oncology are also provided. Given the size of multi-dimensional data sets commonly acquired in imaging studies, care has been taken to maximize computational efficiency and minimize memory usage. All methods are illustrated using both simulated and real-world medical imaging data available in the public domain.

Keywords: contrast, **dcemriS4**, diffusion, dynamic, enhanced, imaging, magnetic, resonance.

1. Introduction

Quantitative analysis of tissue perfusion using dynamic contrast-enhanced magnetic resonance imaging (DCE-MRI) is achieved through a series of processing steps, starting with the raw data acquired from the MRI scanner, and involves a combination of physics, mathematics, engineering and statistics to produce a set of statistical images based on parameter estimates from a compartmental model. The purpose of the **dcemriS4** package is to provide the user with a collection of functions and subroutines that move experimental data through all steps of this data analysis pipeline (Whitcher and Schmid 2011), using standard data formats (such as ANALYZE or NIFTI) that may be visualized and manipulated in R (R Development Core Team 2011) or exported for accessibility across a wide variety of medical image analysis software packages.

The S4 designation in **dcemriS4** means that S4 object classes are used throughout to ensure efficient and transparent manipulation of ANALYZE or NIFTI data structures. Data input and output rely upon the **oro.nifti** package (Whitcher *et al.* 2011; Tabelow *et al.* 2011). Pa-

parameter estimates in **dcemriS4** inherit attributes from the incoming ANALYZE/NIfTI objects in order to preserve anatomical and physiological information for appropriate visualization in R or other software packages. All functions for parameter estimation may also be applied to aggregated data; i.e., a mean curve across an anatomical region of interest. However, the methodology presented here is intended to be applied on a voxel-by-voxel basis to the ANALYZE or NIfTI objects and all statistical summaries are output as valid NIfTI objects to facilitate interoperability. As voxel-wise quantitative analysis can be time consuming, **dcemriS4** supports basic parallel computing by incorporating the **parallel** package. Computations are easily parallelized with the variable `multicore=TRUE` in the most computationally expensive functions.

2. Dynamic contrast-enhanced magnetic resonance imaging

While initial application of DCE-MRI was in the characterization of blood-brain barrier (BBB) integrity (Tofts and Kermode 1984; Larsson *et al.* 1990; Larsson and Tofts 1992), we will instead focus on the application of DCE-MRI to the quantitative analysis of tumor perfusion in oncology. Angiogenesis, the creation of new capillaries from existing blood vessels, and vasculogenesis, the *de novo* generation of blood vessels, are key biological processes that supply nutrients to tissue (Collins and Padhani 2004). New drug therapies, such as antiangiogenic or vaccine therapies, are expected to be cytostatic (i.e., inhibiting or suppressing cellular growth) and may not produce changes in tumor size as measured by traditional structural imaging techniques (Choyke *et al.* 2003). Thus, the ability to study malignant vasculature through non-invasive MRI methods is advantageous. We will cover a DCE-MRI data analysis pipeline using **dcemriS4** that is fully quantitative and produces biologically-relevant parameter estimates from a compartmental model. The interested reader will find several chapters in Jackson *et al.* (2005) and Parker and Padhani (2003) pertaining to the scientific background, methodology and application of DCE-MRI.

The acquisition protocol for a DCE-MRI scan involves several steps. Conversion of signal intensity to contrast agent concentration requires the preliminary step of estimating the T1 relaxation value of the tissue; e.g., using multiple flip-angles or inversion recovery (Bernstein *et al.* 2004). For higher field strengths one may also consider characterizing the inhomogeneity of the magnetic field in the scanner. The dynamic set of T1-weighted images are started approximately 30 – 60 seconds before a bolus injection of the low molecular weight contrast agent – a gadolinium chelate – and continue for 8 – 12 minutes in oncology studies. The length of the dynamic acquisition may easily exceed one hour when characterizing the integrity of the blood brain barrier. Temporal sampling rates depend on multiple factors: type of cancer, anatomy, spatial resolution, spatial coverage, field strength of the scanner, breathing method, etc. and must be carefully considered on a study-by-study basis. DCE-MRI relies on the reduction in T1 relaxation time, corresponding to positive signal enhancement, caused by the presence of the contrast agent. The quantitative analysis of DCE-MRI data in **dcemriS4** consists of the following steps

1. Pre-processing of the T1 signal (e.g., motion correction, co-registration, correction of the B1 field) is introduced in Sections 2.1 and 2.2,
2. Estimation of voxel-wise contrast agent concentration time curves is introduced in Section 2.3,

3. Determination of the arterial input function (AIF), either from the literature or by data-driven methods, is introduced in Section 2.4,
4. Parameter estimation for a given compartmental model is introduced in Section 2.5, and
5. Statistical inference on kinetic parameters for differences between scans of a single patient or between distinct patients, is discussed in Section 2.6.

2.1. Motion correction and co-registration

Basic motion correction within an acquisition, and co-registration between acquired series, is available using the `ftm` function for fast template matching (Lewis 1995). A reference volume must be pre-specified where a mask has been applied to remove all voxel that should not be included in the algorithm. Note, only three-dimensional translations are allowed and no interpolation is used (i.e., only whole-voxel translations) at this time. More sophisticated image registration methodology in R is being developed in the **RNiftyReg** package (Clayden 2011). Access to the image registration routines from the Insight Toolkit (ITK, <http://www.itk.org>) is highly desirable and currently under investigation.

2.2. B1 mapping via the saturated double-angle method

For *in vivo* MRI at high field (≥ 3 Tesla) it is essential to consider the homogeneity of the active B1 field (B1+). The B1 field is the magnetic field created by the radio frequency coil passing an alternating current at the Larmor frequency. The B1+ field is the transverse, circularly polarized component of B1 that is rotating in the same sense as the magnetization. When exciting large collections of spins, non-uniformity in B1+ results in nonuniform treatment of spins. This leads to a spatially varying signal and contrast, and to difficulty in image interpretation and quantification (Cunningham *et al.* 2006).

The proposed method uses an adaptation of the double angle method (DAM). Such methods allow calculation of a flip-angle map, which is an indirect measure of the B1+ field. Two images are acquired: I_1 with prescribed angle α_1 and I_2 with prescribed angle $\alpha_2 = 2\alpha_1$. All other signal-affecting sequence parameters are kept constant. For each voxel, the ratio of magnitude images satisfies

$$\frac{I_2(r)}{I_1(r)} = \frac{\sin \alpha_2(r) f_2(T1, TR)}{\sin \alpha_1(r) f_1(T1, TR)} \quad (1)$$

where r represents spatial position and $\alpha_1(r)$ and $\alpha_2(r)$ are flip angles that vary with the spatially varying B1+ field. If the effects of T1 and T2 relaxation can be neglected, then the actual flip angles as a function of spatial position satisfy

$$\alpha(r) = \arccos \left(\left| \frac{I_2(r)}{2I_1(r)} \right| \right) \quad (2)$$

A long repetition time ($TR \geq 5 \cdot T1$) is typically used with double-angle methods so that there is no T1 dependence in either I_1 or I_2 ; i.e., $f_1(T1, TR) = f_2(T1, TR) = 1$. Instead, the proposed method includes a magnetization-reset sequence after each data acquisition with the goal of putting the spin population in the same state regardless of whether the α_1 or α_2 excitation was used for the preceding acquisition.

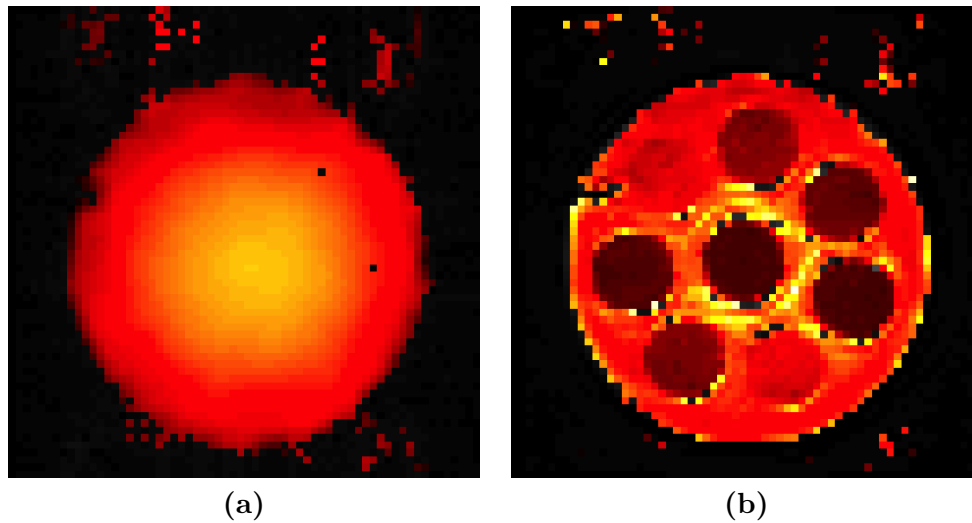


Figure 1: **(a)** Estimated B1+ field (with isotropic Gaussian smoothing) using the saturated double-angle method. The colors correspond to a multiplicative factor relative to the true flip angle (60°). **(b)** Estimated T1 relaxation rates for the phantom data acquisition. The colormap covers the range $[0, 2.5]$ sec.

Example using phantom data

Using data acquired from a T1 phantom at two flip angles, $\alpha_1 = 60^\circ$ and $\alpha_2 = 120^\circ$, we compute the multiplicative factor relative to the low flip angle using the saturated double-angle method (Cunningham *et al.* 2006). Note, repeated acquisitions (five) of each flip angle were obtained and force the additional `rowMeans` step to average the results from the function `doubleAngleMethod` in the code below.

```
R> f60 <- system.file(file.path("nifti", "SDAM_ep2d_60deg_26slc.nii.gz"),
+                      package="dcemriS4")
R> sdam60 <- readNIfTI(f60)
R> f120 <- system.file(file.path("nifti", "SDAM_ep2d_120deg_26slc.nii.gz"),
+                      package="dcemriS4")
R> sdam120 <- readNIfTI(f120)
R> sdam.image <- rowMeans(doubleAngleMethod(sdam60, sdam120, 60), dims=3)
R> mask <- (rowSums(sdam60, dims=3) > 64)

R> # A smooth version of "sdam.image"
R> fsmooth <- system.file(file.path("nifti", "SDAM_smooth.nii.gz"),
+                          package="dcemriS4")
R> SDAM <- readNIfTI(fsmooth)
R> overlay(sdam120, ifelse(mask, SDAM, NA), z=13, zlim.x=range(sdam120),
+          zlim.y=c(0.5,1.5), plot.type="single")
R> par(cex=4,col="white")
```

Three-dimensional isotropic smoothing should be applied before using this field to modify flip angles associated with additional acquisitions; e.g., in the **AnalyzeFMRI** package (Marchini

and Lafaye de Micheaux 2009; Tabelow *et al.* 2011). Figure 1a is the estimated B1+ field (with isotropic Gaussian smoothing) for a gel-based phantom containing a variety of T1 relaxation times. The center of the phantom exhibits a flip angle $> 60^\circ$ while the flip angle rapidly becomes $< 60^\circ$ when moving away from the center in either the x , y or z dimensions. The function `overlay` is part of the **oro.nifti** package, additional functions for the visualization of ANALYZE/NIfTI data are `image` (overloaded for classes `nifti` and `anlz`) and `orthographic`. Assuming the smoothed version of the B1+ field has been computed (in the `SDAM` object here), multiple flip-angle acquisitions can be used to estimate the T1 relaxation rate from the subject (or phantom). The multiplicative factor, derived from the saturated double-angle method, is used to produce a spatially-varying flip-angle map and input into the function `R1.fast`.

```
R> alpha <- c(5,10,20,25,15)
R> nangles <- length(alpha)
R> fnames <- file.path("nifti", paste("fl3d_vibe-", alpha, "deg.nii.gz", sep=""))
R> X <- Y <- 64
R> Z <- 36
R> flip <- fangles <- array(0, c(X,Y,Z,nangles))
R> for (w in 1:nangles) {
+   vibe <- readNIfTI(system.file(fnames[w], package="dcemriS4"))
+   flip[,1:nsli(vibe),w] <- vibe
+   fangles[,,,w] <- array(alpha[w], c(X,Y,Z))
+ }
R> TR <- 4.22 / 1000 # in seconds
R> fanglesB1 <- fangles * array(SDAM, c(X,Y,Z,nangles))
R> zi <- 13
R> maskzi <- mask
R> maskzi[,,(! 1:Z %in% zi)] <- FALSE
R> R1 <- R1.fast(flip, maskzi, fanglesB1, TR, verbose=TRUE)

Deconstructing data...
Calculating R10 and M0...
Reconstructing results...
```

```
R> overlay(vibe, 1/R1$R10[,1:nsli(vibe)], z=13, zlim.x=c(0,1024),
+         zlim.y=c(0,2.5), plot.type="single")
```

Figure 1b displays the quantitative T1 map for a gel-based phantom using information from the estimated B1+ field. The horizontal tubes embedded within the phantom cover a range of $T1 \in [350, 1543]$ ms, where shorter T1 relaxation times are darker and longer relaxation times are brighter. By defining regions of interest (ROIs) in FSLView one may construct a mask that separates voxels belonging to the 10 unique gels.

```
R> fpmask <- system.file(file.path("nifti", "t1_phantom_mask.nii.gz"),
+                        package="dcemriS4")
R> t1pmask <- readNIfTI(fpmask)
R> pmask <- nifti(array(t1pmask[,25], dim(t1pmask))) # repeat slice 25
```

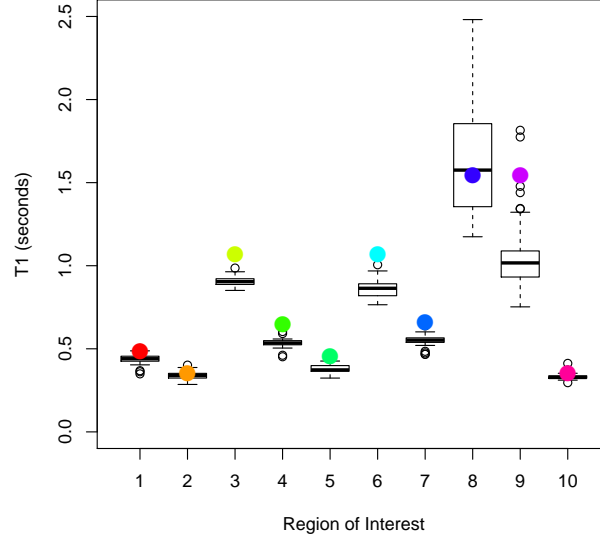


Figure 2: Boxplots of the estimated T1 values for the gel-based phantom, grouped by user-specified regions of interest. True T1 values are displayed as colored circles for each distinct ROI.

We compare the “true” T1 values for each ROI with those obtained from acquiring multiple flip angles with the application of B1+ mapping in Figure 2. Boxplots summarize the estimated T1 relaxation times, across all voxel in the ROI defined by `pmask`, with the true T1 values (large circles). The first seven ROIs correspond to the cylinders that run around and through the phantom, clockwise starting from approximately one o’clock. The eighth and ninth ROIs are taken from the main compartment in the gel phantom; ROI #8 is drawn in the middle of the phantom while ROI #9 is drawn from the outside of the phantom. The final ROI is taken from the central cylinder embedded in the phantom.

2.3. T1 relaxation rate and contrast agent concentration

Estimation of the longitudinal relaxation time T1 is the first step in converting signal intensity, obtained in the dynamic acquisition of the DCE-MRI protocol, to contrast agent concentration (Buckley and Parker 2005). Note, the longitudinal (or spin-lattice) relaxation time T1 is the decay constant of the recovery of the z component of the nuclear spin magnetization towards its thermal equilibrium value (Buxton 2002). Multiple flip-angle acquisitions are commonly used to estimate the intrinsic relaxation rate maps $\{m_0, R_{10}\}$ of the tissue, where m_0 is the equilibrium signal intensity and R_{10} is the pre-injection longitudinal relaxation rate. The non-linear equation

$$S(\theta) = \frac{m_0 \sin(\theta)(1 - E_{10})}{1 - \cos(\theta)E_{10}}, \quad (3)$$

where $E_{10} = \exp(-TR \cdot R_{10})$, relates the observed signal intensity $S(\cdot)$ with the parameters of interest when varying the flip angle θ prior to the injection of the contrast agent. Note, a

repetition time of $TR \approx 4$ ms is common practice for pulse sequences in clinical applications. The Levenberg-Marquardt algorithm, provided in **minpack.lm** (Elzhov *et al.* 2010), is applied to estimate the parameters; see the discussion by Ahearn *et al.* (2005). It is worthwhile to consult known T1 values ($T_{10} = 1/R_{10}$) for different tissue types (e.g., muscle, grey matter, white matter) to ensure the parameter estimates obtained are sensible.

Estimation of the post-injection longitudinal relaxation rate $R_1(t)$ using the time-varying signal intensity $S(t)$ from pre- and post-contrast acquisitions is performed via

$$A(t) = \frac{S(t) - S(0)}{m_0 \sin(\theta)} \quad (4)$$

$$B = \frac{1 - E_{10}}{1 - \cos(\theta)E_{10}} \quad (5)$$

$$R_1(t) = -\frac{1}{TR} \cdot \ln \left\{ \frac{1 - [A(t) + B]}{1 - \cos(\theta)[A(t) + B]} \right\}, \quad (6)$$

where the flip angle $\theta \in [10^\circ, 30^\circ]$ is common for the dynamic acquisitions, but will depend on both the field strength of the magnet and the anatomical region of interest.

The function **R1.fast** (embedded within **CA.fast**) rearranges the multi-dimensional structure of the multiple flip-angle acquisitions into a single matrix, to take advantage of internal R functions instead of loops, and calls **E10.lm** to perform the non-linear regression using the Levenberg-Marquardt algorithm. If only two flip angles have been acquired it is possible to use the function **CA.fast2**, where a linear approximation is applied to estimate the parameters (Wang *et al.* 1987).

The final step of the conversion of the dynamic signal intensities to contrast agent concentration, using the **CA.fast** function, is performed via

$$C_t(t) = \frac{1}{r_1} \left(\frac{1}{T_1} - \frac{1}{T_{10}} \right), \quad (7)$$

where r_1 is the spin-lattice relaxivity constant (depends on the gadolinium chelate and magnet field strength) and $T_{10} = 1/R_{10}$ is the spin-lattice relaxation time in the absence of contrast media (Buckley and Parker 2005). For computational reasons we follow the method of Li *et al.* (2000).

2.4. Arterial input function

Whereas quantitative PET (positron emission tomography) studies routinely perform arterial cannulation on the subject in order to characterize the arterial input function (AIF) directly, it has been common to use literature-based AIFs in the quantitative analysis of DCE-MRI. Examples include

$$C_p(t) = D (a_1 e^{-m_1 t} + a_2 e^{-m_2 t}), \quad (8)$$

where $D = 0.1$ mmol/kg, $a_1 = 3.99$ kg/l, $a_2 = 4.78$ kg/l, $m_1 = 0.144$ min⁻¹ and $m_2 = 0.0111$ min⁻¹ (Weinmann *et al.* 1984; Tofts and Kermode 1984); or $D = 1.0$ mmol/kg, $a_1 = 2.4$ kg/l, $a_2 = 0.62$ kg/l, $m_1 = 3.0$ and $m_2 = 0.016$ (Fritz-Hansen *et al.* 1996). There has been progress in measuring the AIF using the dynamic acquisition and fitting a parametric model to the observed contrast agent concentration time curves. Recent models include a mixture

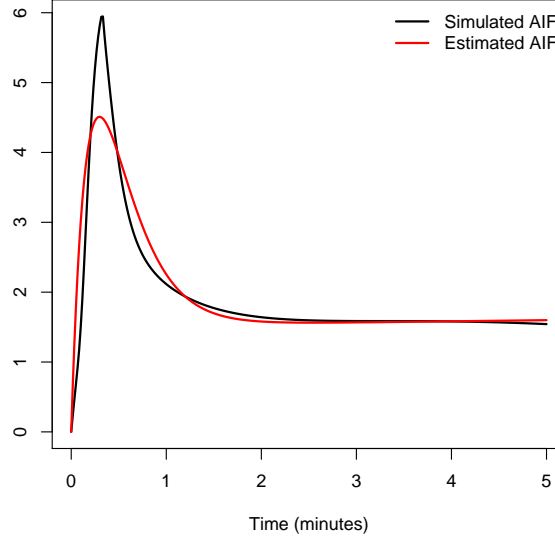


Figure 3: Simulated arterial input function (AIF) from Buckley (2002) and the best parametric fit using the sums-of-exponentials model in Orton *et al.* (2008).

of Gaussians (Parker *et al.* 2006) and sums of exponentials (Orton *et al.* 2008). The **dcemriS4** package has incorporated the sums-of-exponentials model

$$C_p(t) = A_B t e^{-\mu_B t} + A_G (e^{-\mu_G t} + e^{-\mu_B t}) \quad (9)$$

(Orton *et al.* 2008), where the unknown parameters $\beta = (A_B, \mu_B, A_G, \mu_G)$ are estimated using nonlinear regression. Using the AIF defined in Buckley (2002), we illustrate fitting a parametric model to characterize observed data. The `orton.exp.lm` function provides this capability using the so-called double-exponential parametric form `orton.exp` (9).

```
R> data("buckley")
R> aifparams <- with(buckley, orton.exp.lm(time.min, input))
R> fit.aif <- with(aifparams,
+               aif.orton.exp(buckley$time.min, AB, muB, AG, muG))
```

Figure 3 shows both the true AIF and the best parametric description using a least-squares fitting criterion. It is apparent from the figure that the sums-of-exponentials model cannot match the underlying AIF from the simulated data. This illustrates an inherent deficiency in parametric models regardless of their application – the fact that it may not be appropriate to describe the true process.

2.5. Kinetic parameter estimation

The focus in this section is fully quantitative pharmacokinetic modeling of tissue perfusion and assumes the raw scanner data has been converted to contrast agent concentration. Please see Collins and Padhani (2004) and Buckley and Parker (2005) for discussions on this point.

The standard Kety model (Kety 1960), a single-compartment model, and the extended Kety model, the standard Kety model with an extra “vascular” term, form the collection of basic parametric models one can apply using **dcmriS4**. Regardless of which parametric model is chosen for the biological system, the contrast agent concentration time curve at each voxel in the region of interest (ROI) is approximated using the convolution of an AIF and the compartmental model; i.e.,

$$C_t(t) = K^{\text{trans}} \left[C_p(t) \otimes e^{-k_{\text{ep}}t} \right], \quad (10)$$

$$C_t(t) = v_p C_p(t) + K^{\text{trans}} \left[C_p(t) \otimes e^{-k_{\text{ep}}t} \right]. \quad (11)$$

The K^{trans} parameter represents the volume transfer constant between the plasma and the extravascular extracellular space (EES) per minute, and k_{ep} is the rate constant between EES and blood plasma. The parameter v_p , in the so-called “extended” Kety model (11), describes the fraction of contrast agent in the plasma, while

$$v_e = \frac{K^{\text{trans}}}{k_{\text{ep}}} \quad (12)$$

is the fraction of the contrast agent in the EES.

Parameter estimation may be performed using one of four options in the current version of this software:

1. **dcmri.lm**: Non-linear regression using non-linear least squares (Levenberg-Marquardt optimization),
2. **dcmri.map**: Bayesian *maximum a posteriori* (MAP) estimation (Nelder-Mead algorithm)
3. **dcmri.bayes**: Fully Bayesian inference using Markov chain Monte Carlo (MCMC) (Schmid *et al.* 2006),
4. **dcmri.spline**: Deconvolution via non-parametric curve fitting using Bayesian penalized splines (with MCMC) (Schmid *et al.* 2009b).

Non-linear regression

Least-square estimates of the kinetic parameters ($K^{\text{trans}}, k_{\text{ep}}$), also for v_p for the extended Kety model, are provided in **dcmri.lm**. In each voxel a nonlinear regression model is applied to the contrast agent concentration time curves. All convolutions between compartmental models and AIFs are evaluated analytically to increase computational efficiency. For example, the convolution in (10) with the literature-based AIF (8) produces a statistical model that is given by

$$C_t(t) = D \exp(\theta_1) \sum_{i=1}^2 \frac{a_i \{ \exp(-m_i t) - \exp[-\exp(\theta_2)t] \}}{\exp(\theta_2) - m_i} + \epsilon(t), \quad (13)$$

where $\epsilon(t)$ is the observational error at time t , $\theta_1 = \log(K^{\text{trans}})$ and $\theta_2 = \log(k_{\text{ep}})$. The parametrization (θ_1, θ_2) is used instead of $(K^{\text{trans}}, k_{\text{ep}})$ to ensure positive values for both transfer rates. We assume the expected value of the noise term to be zero; i.e., $E(\epsilon) = 0$. Inference

is performed by minimizing the sum of squares of the observational errors $\min_{\theta} \{\sum_t [\epsilon(t)]^2\}$. The parameter v_e is calculated using (12).

Model parameters are estimated, along with asymptotic standard errors, using the Levenberg-Marquardt algorithm (Moré 1978) in **minpack.lm**. Note, for the typical number of time points used in DCE-MRI, the estimation procedure is not well-behaved asymptotically and, thus, the asymptotic standard errors are not accurate (Schmid *et al.* 2006).

Bayesian model

A hierarchical Bayesian model can be described in three stages: the data model, the process model and the prior parameters.

1. For the *data model* we assume a signal-plus-noise model; such that the observed concentration of contrast agent $C_t(t)$ in a single voxel at time point t with additive Gaussian error variance σ^2 , is given by

$$C_t(t) \sim N(f(K^{\text{trans}}, k_{\text{ep}}, t), \sigma^2). \quad (14)$$

This is the Bayesian analogue to the application of the least-squares fitting method in the non-linear regression approach.

2. For the *process model* we use the single-compartment model (10) or an extended Kety model (11). Evaluating the convolution for the single-compartment model produces

$$f(K^{\text{trans}}, k_{\text{ep}}, t) = DK^{\text{trans}} \sum_{i=1}^2 \frac{a_i [\exp(-m_i t) - \exp(-k_{\text{ep}} t)]}{k_{\text{ep}} - m_i}. \quad (15)$$

As previously discussed, the kinetic parameters K^{trans} and k_{ep} are transfer rates and must remain positive. Gaussian priors on their logarithmic transforms

$$\log(K^{\text{trans}}) \sim N(a(K^{\text{trans}}), b(K^{\text{trans}})), \quad (16)$$

$$\log(k_{\text{ep}}) \sim N(a(k_{\text{ep}}), b(k_{\text{ep}})), \quad (17)$$

ensure this constraint is met. In breast tissue, for example, reasonable priors for both parameters should not exceed values of approximately 20 min^{-1} (Schmid *et al.* 2006). Hence, we use parameters $a(K^{\text{trans}}) = a(k_{\text{ep}}) = 0$ and $b(K^{\text{trans}}) = b(k_{\text{ep}}) = 1$. Thus, the expected value of K^{trans} and k_{ep} is one, and with 99.86% probability *a priori* neither kinetic parameter will exceed 20 min^{-1} . For scans covering other tissue types, the hyperparameters $a(K^{\text{trans}}), b(K^{\text{trans}})$ and $a(k_{\text{ep}}), b(k_{\text{ep}})$ may be adjusted accordingly when calling **dcemri.bayes**. In case of the “extended” Kety model, a Beta prior with parameters $a(v_p)$ and $b(v_p)$ is used for the vascular fraction v_p , with *a priori* expected value $E(v_p) = a(v_p)/[a(v_p) + b(v_p)]$.

3. For the *prior parameter*, in this case the variance of the observational error, we apply a flat inverse Gamma prior

$$\sigma^2 \sim IG(a(\sigma^2), b(\sigma^2)), \quad (18)$$

with default parameters $a(\sigma^2) = 1$ and $b(\sigma^2) = 0.001$ that reflect our lack of prior information.

The three stages of the hierarchical model fully specify our *a priori* knowledge. To combine this with the observed data and produce *a posteriori* knowledge, we apply Bayes' theorem

$$\pi(\mathbf{h} | C_t) = \frac{\pi(\mathbf{h}) \ell(C_t | \mathbf{h})}{\int \pi(\mathbf{h}^*) \ell(C_t | \mathbf{h}^*)}, \quad (19)$$

where $\mathbf{h} = (K^{\text{trans}}, k_{\text{ep}}, \sigma^2)$ denotes the vector of all parameters across all voxel, $\pi(\mathbf{h})$ the product of the prior PDFs and $\ell(C_t | \mathbf{h})$ denotes the (Gaussian) likelihood function of $C_t(t)$ from (14). In the Bayesian framework, conclusions are drawn from the joint posterior PDF only. Two functions are provided to exploit the posterior PDF:

- The function `dcmri.map` provides voxel-wise *maximum a posteriori* (MAP) estimators (DeGroot 1970) using the Nelder-Mead algorithm provided in `optim`. Note, the posterior may be multi-modal and, hence, a global optimization may not be appropriate and/or feasible. No standard errors are provided with this method.
- The function `dcmri.bayes` provides the posterior median as the summary statistic for $(K^{\text{trans}}, k_{\text{ep}}, v_p)$, along with the posterior standard deviation for all statistics, by sampling from the posterior using MCMC (Gilks *et al.* 1996). All samples from the joint posterior distribution may be saved using the option `samples=TRUE`, allowing one to interrogate the posterior probability density function (PDF) of all parameter estimates. To increase computational efficiency sampling from the posterior distribution is implemented in C and linked to R. It is useful to retain all samples from the joint posterior when one wants to construct, for example, voxel-wise credible intervals on the kinetic parameters. The algorithm is computationally expensive and parallel computation has been enabled with the `parallel` package by setting the option `multicore=TRUE`.

Bayesian penalized splines

An alternative to parametric modeling, the function `dcmri.spline` may be used to deconvolve and de-noise the contrast agent concentration time curves using an adaptive penalized spline approach (Schmid *et al.* 2009b). A Bayesian hierarchical model is constructed

1. The *data model* is the Gaussian observation model (14).
2. For the *process model* a general approach is used, such that

$$f(t) = C_p(t) \otimes R(t), \quad (20)$$

where $R(t)$ is the response function in the tissue. The convolution is derived through the discretization of $C_p(t)$ and $R(t)$ (e.g., at the observation time points), allowing one to use the observed AIF instead of a parametric model. The response is assumed to be a smooth function, modeled as an adaptive penalized spline

$$R(t) = \sum_{j=1}^p \beta_j B_j(t), \quad (21)$$

where \mathbf{B} is a B -spline design matrix. An adaptive second-difference penalty is used on the spline regression parameters β_j ; i.e.

$$\beta_j = 2\beta_{j-1} - \beta_{j-2} + e_j \quad j = 3, \dots, p, \quad (22)$$

where $e_j \sim N(0, \delta_i^2)$. Note, a first-order penalty is also available using the option `rw=1`.

3. The *prior* for the adaptive smoothing parameter δ_i^2 is given by

$$\delta_i^2 \sim IG(a(\delta), b(\delta)) \quad (23)$$

with default parameters $a(\delta) = b(\delta) = 10^{-5}$ that provide nearly flat prior information, and an Inverse Gamma prior for the observational error (18).

Making use of Bayes' formula (19), the posterior is assessed using an MCMC algorithm. By default, the function `dcemri.spline` returns the median of the maximum F_p of the response function $R(t)$ per voxel. The median response function (`response=TRUE`) and the fitted contrast agent concentration time curve (`fitted=TRUE`) may also be provided.

An automated method for estimation of the onset time of contrast agent (from a bolus injection) has been implemented. The algorithm follows these steps:

1. Find the minimum time t , for which the contrast agent concentration curve significantly exceeds zero,
2. Compute the gradient of C_t at point t , exploiting the derivative of the B -spline,
3. Compute the onset time as

$$t_0 = t - \frac{C_t(t)}{dC_t(t)/dt}. \quad (24)$$

To provide estimates of the kinetic parameters from a compartmental model, a parametric model may be applied to the estimated response curve (`nlr=TRUE`). At this point in time a single exponential model ("`weinmann`") or the adiabatic approximation to the tissue homogeneity model ("`AATH`") are available. For the AATH model, the response function is given by

$$R(t) = F_p \cdot \begin{cases} E \exp[-(t - T_c) EF_p/v_e] & \text{for } t \geq T_c, \\ 0 & \text{for } t < 0, \\ 1 & \text{for } 0 \leq t < T_c, \end{cases} \quad (25)$$

where T_c is the transit time through the capillary, E is the extraction fraction and F_p is the mean plasma flow. These parameters may be re-expressed as the kinetic parameters from the (extended) Kety model via

$$K^{\text{trans}} = EF_p, \quad (26)$$

$$k_{\text{ep}} = EF_p/v_e, \quad (27)$$

$$v_p = T_c F_p. \quad (28)$$

The response model is applied to each sample of the estimated response curve, and the median and standard error of the kinetic parameters are provided. Samples from the posterior

density for the kinetic parameters, the maximum response F_p , the onset time t_0 , the response functions, and the fitted curves are also available (`samples=TRUE`). Parallel computing may be accessed using the **parallel** package (`multicore=TRUE`).

Estimating the kinetic curves

Using kinetic parameters estimated with one of the methods above, the functions `kineticModel` or `orton.exp.lm` may be used to compute the estimated contrast agent concentration time curves for the given parametric models. A list of arrays or `nifti` class objects of kinetic parameters can be given to `kineticModel` to produce voxel-wise estimates of the compartmental model.

2.6. Statistical inference

No specific support is provided for hypothesis testing in **dcmriS4**. We recommend one uses built-in functions in R to perform ANOVA (analysis of variance) or mixed-effects models based on statistical summaries of the kinetic parameters over a given ROI on a per subject per visit basis. An alternative to this traditional approach is to analyze an entire study using a Bayesian hierarchical model (Schmid *et al.* 2009a), where an implementation is under development in the software project **PILFER** (<http://pilfer.sourceforge.net>). One may also question the rationale for hypothesis testing in only one kinetic parameter. Preliminary work has been performed in looking at the joint response to treatment of both K^{trans} and k_{ep} in DCE-MRI using functional data analysis (O'Connor *et al.* 2010).

3. Diffusion weighted imaging

Diffusion weighted imaging (DWI) is an imaging biomarker that is rapidly becoming popular and widely applied in oncology (Chenevert *et al.* 2002; Koh and Padhani 2006). DWI allows one to quantify the diffusion behavior of water by estimating the apparent diffusion coefficient (ADC) (Wheeler-Kingshott *et al.* 2003). That is, assuming completely unrestricted motion of water, how is the motion of water impeded by the biological structure of tissue? The reduction in the ability of water to diffuse in tissue has been used to infer biologically-relevant information in oncology; e.g., in tumor detection, disease progression and the evaluation of treatment response.

DWI is an MR technique that provides a unique insight into tissue structure through MRI diffusion measurements *in vivo* (Moseley *et al.* 1990; Wheeler-Kingshott *et al.* 2003). These diffusion measurements reflect the effective displacement of water molecules allowed to migrate for a given time (Le Bihan *et al.* 1988). Using the Stejskal–Tanner equation

$$S = S_0 \exp(-\gamma^2 G^2 \delta^2 (\Delta - \delta/3) D) = S_0 \exp(-bD), \quad (29)$$

one may solve for the unknown diffusion to obtain the *apparent diffusion coefficient* (ADC) D (Wheeler-Kingshott *et al.* 2003). For completeness, S_0 is the (unknown) signal intensity without the diffusion weighting, S is the observed signal with the gradient applied, γ is the gyromagnetic ratio, G is the strength of the gradient pulse, δ is the duration of the gradient pulse and Δ is the time between the two pulses. The micro-parameters $(\gamma, G, \Delta, \delta)$ are selected prior to data acquisition and may be combined into a single parameter $b = \gamma^2 G^2 \delta^2 (\Delta - \delta/3)$,

known as the b -value. The functions `ADC.fast` and `adc.lm` perform parameter estimation using a similar interface to kinetic parameter estimation previously introduced for DCE-MRI with the Levenberg-Marquardt algorithm.

Acquisition protocols typically involve obtaining a volume without diffusion weighting ($b = 0$ s/mm²), at low diffusion weighting ($b \geq 100$ s/mm²) and higher diffusion weighting ($b \geq 500$ s/mm²). When estimating the ADC value, one should exclude any acquisitions with $b \leq 100$ s/mm² to minimize the influence of perfusion effects (Padhani *et al.* 2009).

The diffusivity of water at room temperature without restrictions is approximately 3.0×10^{-3} mm²/s. Once the ADC is estimated in the tissue of interest at baseline, treatment response may be assessed at subsequent time points. The most appropriate timings depend on both the type of tumor and treatment regime. Observing an decrease in diffusivity, via a decrease in the ADC values post-treatment, may be a result of cell swelling after initial chemotherapy or radiotherapy followed by an increase in diffusivity, via an increase in the ADC values, from cell necrosis and lysis. A decrease in ADC values may be observed directly through tumor apoptosis after treatment (Koh and Padhani 2006; Padhani *et al.* 2009).

4. The RIDER Neuro MRI data repository

The National Biomedical Imaging Archive (NBIA; <http://cabig.nci.nih.gov/tools/NCIA>) is a searchable, national repository integrating *in vivo* cancer images with clinical and genomic data. The NBIA provides the scientific community with public access to DICOM images, image markup, annotations, and rich metadata. The DCE-MRI and DW-MRI data analyzed here were downloaded from the “RIDER Neuro MRI” collection (<http://wiki.nci.nih.gov/display/CIP/RIDER>).

4.1. Dynamic contrast-enhanced MRI

Functions of the **oro.nifti** package are utilized to read the signal intensity files, in ANALYZE or NIFTI format, obtained from the MRI scanner (after conversion from DICOM). In this example pre-contrast multiple flip angle acquisitions are available for estimation of contrast agent concentration. We use `CA.fast` to estimate the intrinsic relaxation rate R_{10} and equilibrium signal intensity m_0 from (3) and the contrast agent concentration curve $C_t(t)$ from (7). In order to save computation time and memory, we utilize a binary mask with a very limited region-of-interest (ROI) created in FSLView (<http://fsl.fmrib.ox.ac.uk/fsl/fslview/>) and saved in ANALYZE format.

```
R> perf <- paste("281949", "19040721", "perfusion.nii.gz", sep="_")
R> fmask <- system.file(file.path("nifti", sub(".nii", "_mask.hdr", perf)),
+                       package="dcemriS4")
R> mask <- readANALYZE(fmask)
R> mask <- ifelse(mask > 0, TRUE, FALSE)
R> dynamic <- readNIfTI(perf)

R> TR <- 4.43 / 1000 # taken from CSV file
R> dangle <- 25      # taken from CSV file
R> (fflip <- list.files(pattern="ax[0-9]"))
```

```

R> (fangles <- as.numeric(sub(".*ax([0-9]+).*", "\\1", fflip)))
R> flip <- array(NA, c(dim(mask), length(fangles)))
R> for (fa in 1:length(fangles)) {
+   flip[,,,fa] <- readNIfTI(fflip[fa])
+ }

R> ca <- CA.fast(dynamic, mask, dangle, flip, fangles, TR)
R> writeNIfTI(ca$M0, paste(perf, "m0", sep="_"))
R> writeNIfTI(ca$R10, paste(perf, "r10", sep="_"))
R> writeNIfTI(ca$conc, paste(perf, "gdconc", sep="_"))

```

Note, we have used information in the file names to provide the flip angles (`fangles`) for input into `CA.fast` ensuring that the flip angles match the flip-angle array (`flip`). After estimating the contrast agent concentration time curve in each voxel we fit a compartmental model to obtain estimates of the kinetic parameters that describe the simplified biological process of perfusion. Here, the “extended” Kety model is used, which includes a vascular compartment. An AIF must be defined in order to complete the compartmental model in (11). It is relatively straightforward to estimate such an AIF from contrast agent concentration time curves from an appropriate voxel or collection of voxels. However, for simplicity we select a literature-based AIF, the sum of two exponentials with values taken from [Fritz-Hansen *et al.* \(1996\)](#), that is available for all compartmental model fitting procedures.

Non-linear regression

A numeric optimization of the least-square criterion, using the Levenberg-Marquardt algorithm, is provided by `dcmri.lm` and illustrated below. Note that the acquisition times for the dynamic series are read in from a pre-existing text file, converted from seconds to minutes (using `str2time` from `oro.dicom`) and offset by the bolus injection time (at the ninth acquisition). This information was obtained from the original DICOM data and saved in `rawtimes.txt`. The literature-based AIF `fritz.hansen` is used here for illustrative purposes. Alternatives include estimating values for a parametric AIF (e.g., `aif="orton.exp"`) from the data and supplying them via the `user` option in `dcmri.lm`, or providing an empirical AIF (`aif="empirical"`) and passing the vector of AIF values via the `user` option.

```

R> acqtimes <- str2time(unique(sort(scan("rawtimes.txt", quiet=TRUE))))$time
R> acqtimes <- (acqtimes - acqtimes[9]) / 60 # minutes
R> conc <- readNIfTI(paste(perf, "gdconc", sep="_"))

R> fit.lm <- dcmri.lm(conc, acqtimes, mask, model="extended",
+                   aif="fritz.hansen", control=nls.lm.control(maxiter=100),
+                   multicore=TRUE, verbose=TRUE)
R> writeNIfTI(fit.lm$ktrans, paste(perf, "ktrans", sep="_"))

R> overlay(dynamic, ifelse(mask, fit.lm$ktrans, NA), w=11, zlim.x=c(32,256),
+          zlim.y=c(0,0.1))

```

Figure 4 shows the estimated K^{trans} statistical images in the pre-defined ROI overlaid on the dynamic acquisition (for anatomical reference). Two rings of high K^{trans} values are visually

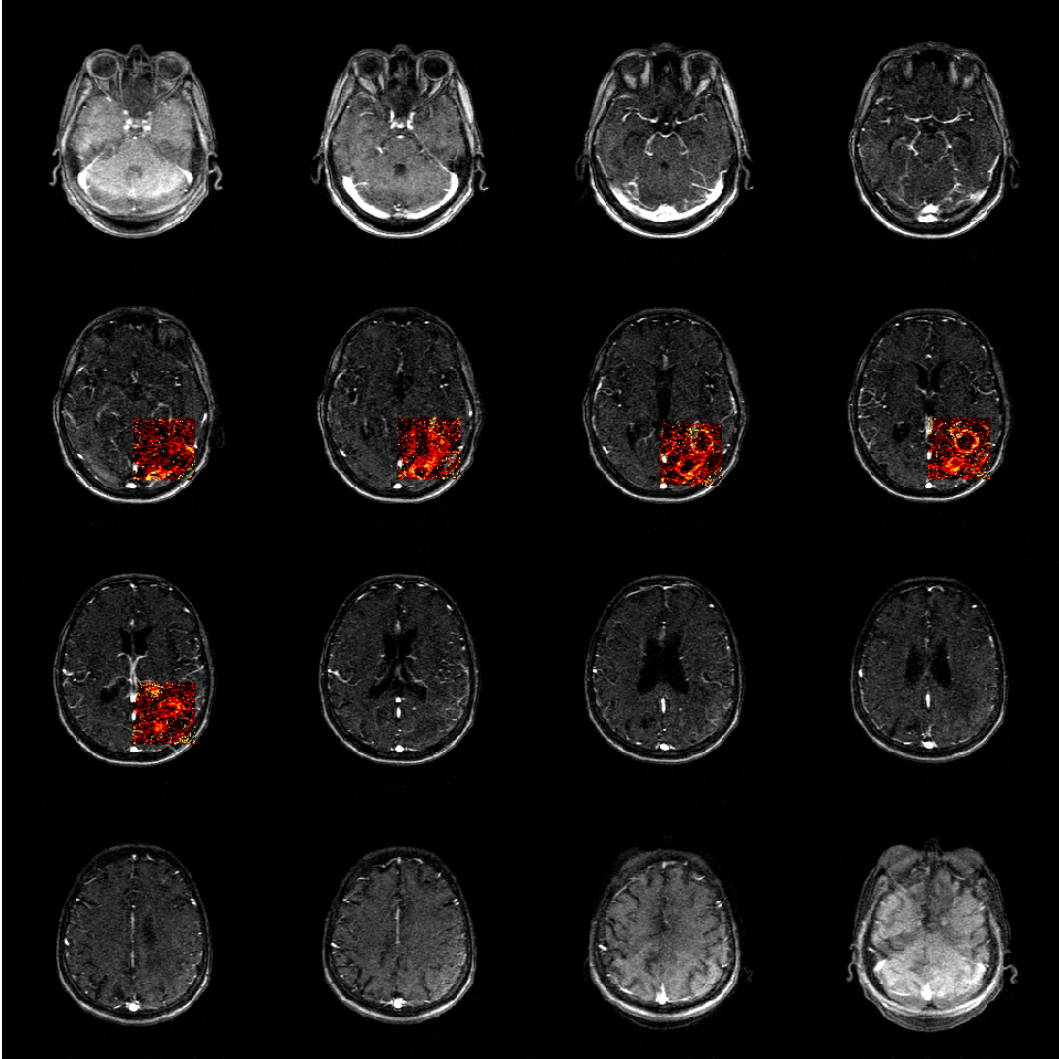


Figure 4: Statistical images of K^{trans} overlaid on the dynamic acquisition for the RIDER Neuro MRI data. Two potential tumors are visible, in the region-of-interest, by enhanced rims of high K^{trans} and central cores of low K^{trans} . The values of K^{trans} are $[0, 0.1] \text{ min}^{-1}$.

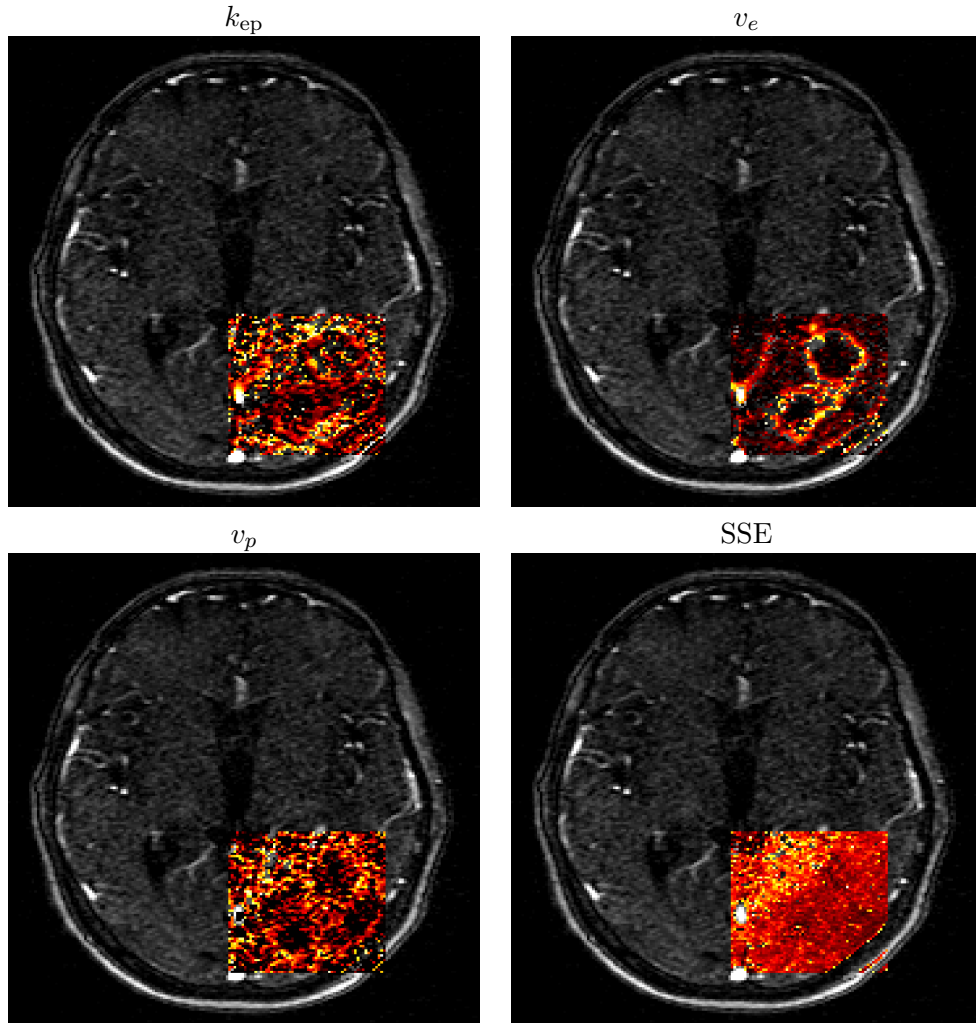


Figure 5: Statistical images of the RIDER Neuro MRI data using non-linear regression for slice $z = 7$. The parameter k_{ep} is the rate constant between EES and blood plasma (units are $[0, 1.25] \text{ min}^{-1}$), v_p is the vascular space fraction of plasma (units are $[0, 30] \%$) and v_e is the EES space fraction (units $[0, 30] \%$). The sums-of-squared error (SSE) measures the quality of fit over the tumor region-of-interest (units are $[0, 0.05]$).

apparent from the statistical images, indicating the presence of two tumors. In both cases K^{trans} is nearly zero in the center of both rings, indicating that no blood is being supplied to the core of the tumors (most likely caused by necrotic or apoptotic processes). Figure 5 provides statistical images that summarize the entire model-fitting procedure for slice $z = 7$. For both tumors the fraction of contrast agent in the extravascular extracellular space (EES) v_e is high at the tumor rim, a common feature in a tumor that is hypervascular compared to the surrounding tissue. The perfusion/permeability is vastly diminished in the core of the tumor, exhibited by low values of k_{ep} and v_p . Goodness-of-fit for the compartmental model may be assessed using the sums-of-squared error (SSE). The SSE over the given ROI covers a variety of tissue types; e.g., white matter, gray matter, cerebrospinal fluid (CSF), skull and air. The SSE is high for tissue types in which the compartmental model is not appropriate. In contrast, the SSE is nearly spatially invariant across the healthy brain tissue and tumor.

Bayesian maximum a posteriori (MAP) estimation

Caution must be exercised when using non-linear regression algorithms, since the Levenberg-Marquardt algorithm used in `dcemri.lm` is *not* guaranteed to converge and is susceptible to noise. More robust results may be achieved by using biologically-relevant prior information in a Bayesian framework (Schmid *et al.* 2006). Two methods for parameter estimation from a Bayesian perspective are implemented in **dcemriS4**. The function `dcemri.bayes` uses Markov Chain Monte Carlo (MCMC) to explore the posterior PDF (Gilks *et al.* 1996) and `dcemri.map` uses numerical optimization to maximize the posterior (DeGroot 1970).

From the non-linear regression analysis of the RIDER Neuro MRI data, it appears that approximately $K^{\text{trans}} \in [0, 0.1]$ and $k_{\text{ep}} \in [0, 1.25]$ (Figure 4). Hence, we use a Gaussian distribution with expected value $a(K^{\text{trans}}) = \log(0.05)$ and variance $b(K^{\text{trans}}) = 1$ on $\log(K^{\text{trans}})$, and a Gaussian distribution with expected value $a(k_{\text{ep}}) = \log(0.7)$ and variance $b(k_{\text{ep}}) = 1$ on $\log(k_{\text{ep}})$ as priors. For v_p , we use the Beta distribution $B(a(v_p) = 1, b(v_p) = 19)$; i.e., the expected value is given by $E(v_p) = 0.05$. Parameter estimation via `dcemri.map` follows a consistent user interface established in `dcemri.lm`.

```
R> fit.map <- dcemri.map(conc, acqtimes, mask, model="extended",
+                       aif="fritz.hansen", ab.ktrans=c(log(0.05),1),
+                       ab.kep=c(log(0.7),1), ab.vp=c(1,19),
+                       multicore=TRUE)
R> writeNIfTI(fit.map$ktrans, paste(perf, "ktrans", "map", sep="_"))
```

Figure 6 shows the K^{trans} statistical image for the slice $z = 7$ obtained using the Bayesian MAP estimator. Estimated values are similar to those obtained using non-linear regression (reproduced in Figure 6 to facilitate a side-by-side comparison). The estimation is similar, but subtly different. For example, by using a biological prior on the kinetic parameters the number of voxels where the MAP estimator does not converge is essentially eliminated when compared with non-linear regression.

Because we have avoided a computationally expensive procedure, the computing times for `dcemri.lm` and `dcemri.map` are roughly the same. However, the MAP estimator does not make use of the complete joint posterior PDF.

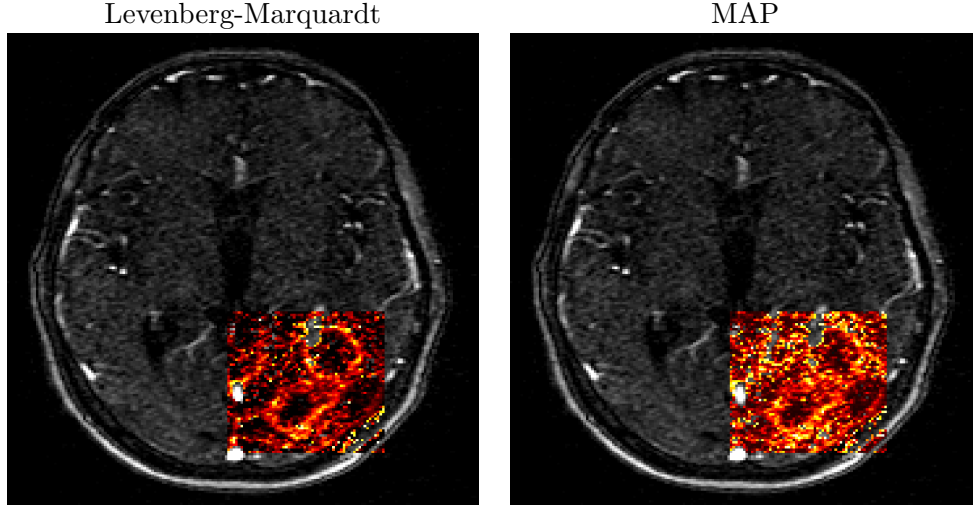


Figure 6: Statistical images of K^{trans} for the RIDER Neuro MRI data (slice $z = 7$). Two methods for parameter estimation are displayed: non-linear regression using the Levenberg-Marquardt algorithm (left) and *maximum a posteriori* (MAP) estimation (right). The values of K^{trans} are $[0, 0.1] \text{ min}^{-1}$ for both images.

Bayesian estimation via Markov Chain Monte Carlo

Using the MCMC algorithm provided by `dcemri.bayes` is computationally expensive when compared with all previous estimation procedures. However, the MCMC algorithm explores the complete posterior PDF. Statistical summaries of the marginal posteriors, associated with all parameters of interest, are provided by default and all samples from the joint posterior may be obtained using the option `samples=TRUE` (internal memory may become an issue when using this option). Using samples from the joint posterior, additional statistics may be derived from the model-fitting procedure; e.g., the reliability of the estimated parameters using credible intervals. The following application of `dcemri.bayes` uses the default `samples=FALSE` and, hence, we are restricted to posterior medians and standard deviations for all parameters in the compartmental model.

```
R> fit.bayes <- dcemri.bayes(conc, acqtimes, mask, model="extended",
+                           aif="fritz.hansen", ab.ktrans=c(log(0.05),1),
+                           ab.kep=c(log(0.7),1), ab.vp=c(1,19))
R> writeNIfTI(fit.bayes$ktrans, paste(perf, "ktrans", "bayes", sep="_"))
```

Figure 7 displays statistical summaries of K^{trans} (posterior median and standard deviation) provided the default settings of `dcemri.bayes`. It is clear that the posterior median differs from the MAP estimator (reproduced in Figure 6 for a side-by-side comparison) across the majority of non-tumor voxel in the ROI. However, K^{trans} values around the enhancing rim of the tumor are similar across all three methods: `dcemri.lm`, `dcemri.map` and `dcemri.bayes`. Figure 7 also provides the posterior standard deviation of K^{trans} and an image of the ratio $\text{sd}(K^{\text{trans}})/\text{median}(K^{\text{trans}})$. Values of $\text{sd}(K^{\text{trans}})$ are higher in areas of large K^{trans} values, even when one adjusts for the estimated $\text{median}(K^{\text{trans}})$. However, $\text{sd}(K^{\text{trans}})$ is quite low



Figure 7: Statistical images of K^{trans} for the RIDER Neuro MRI data (slice $z = 7$) using Bayesian estimation. The posterior median K^{trans} , posterior standard deviation of K^{trans} and the ratio of these two statistics have been obtained from a fully Bayesian MCMC algorithm. The MAP estimator of K^{trans} is also displayed for comparison. The units of K^{trans} are $[0, 0.1] \text{ min}^{-1}$ for both estimation techniques.

overall, usually less than 0.1, in the tumor ROI.

Bayesian penalized splines

An alternative to parametric methods of the biological system is the function `dcmri.spline` where a non-parametric curve is fit to the data using penalized splines (Eilers and Marx 1996; Marx and Eilers 1998). Smoothness of the curve and goodness-of-fit to the data are controlled by two Gamma distributions: a prior for the adaptive smoothness parameters (`ab.hyper`) and a prior for the variance of the observational error (`ab.tauepsilon`). Full details on the methodology for Bayesian penalized P -splines for DCE-MRI are provided in Schmid *et al.* (2009b). For the following application of `dcmri.spline` default values for the hyperparameters have been selected.

```
R> mask.spline <- array(FALSE, dim(mask))
R> z <- 7
R> mask.spline[, , z] <- mask[, , z]
R> fit.spline <- dcmri.spline(conc[, , -(1:8)], acqtimes[-(1:8)], mask.spline,
+                           model="weinmann", aif="fritz.hansen",
+                           multicore=TRUE, nlr=TRUE)
R> writeNIfTI(fit.spline$ktrans, paste(perf, "ktrans", "spline", sep="_"))
R> writeNIfTI(fit.spline$Fp, paste(perf, "Fp", "spline", sep="_"))
```

As a summary statistic the maximum of the response function may be used. Alternatively, a response model may be derived from the response function (`nlr=TRUE`). Please note that a sample of the posterior PDF is given for the response function and, hence, a non-linear fit to the response model is performed for each response function in the sample. The `dcmri.spline` function supports two models, the standard Kety model and the adiabatic approximation of tissue homogeneity (AATH) (St Lawrence and Lee 1998).

Figure 8 depicts the maximum perfusion F_p parameter map for the central tumor slice. Increased perfusion is visible in this image, but overall the quality of the statistical image is poor. This is most likely due to the fact that the acquisition protocol was not optimized for the AATH model, where high temporal resolution is required for accurate parameter estimation. Figure 8 also shows the median K^{trans} parameter map estimated from fitting a Kety response model to the estimated response function. Here, compared to the results above, K^{trans} is slightly increased in the top left area of the ROI due to the negligence of the vascular compartment in the standard Kety model.

4.2. Diffusion weighted imaging

The RIDER Neuro MRI data repository does not provide DWI acquisitions *per se* but a diffusion tensor imaging (DTI) acquisition was performed at each visit. The analysis of DTI data is beyond the scope of this article, but the interested reader is pointed to the following references: Horsfield and Jones (2002); Tofts (2003). The methodology behind DWI and DTI are virtually identical, so we will ignore the extra information provided by a DTI acquisition and analyze the non-directional aspects of the diffusion process here. We acknowledge the fact that the ADC values derived from this DTI acquisition may differ slightly from those estimated using a more common DWI sequence.

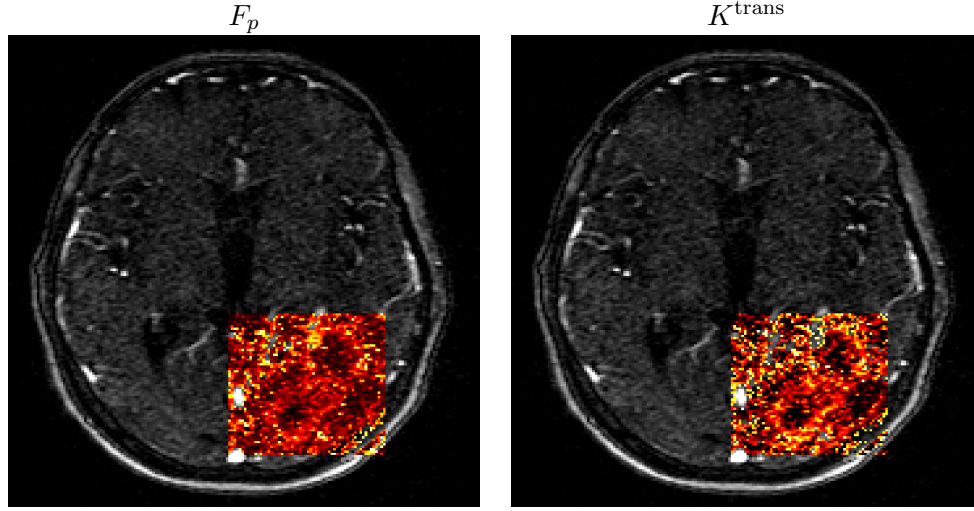


Figure 8: Statistical images of K^{trans} for the RIDER Neuro MRI data (slice $z = 7$) using Bayesian penalized splines. The parameter F_p (left) is given by the maximum of the response function after deconvolution using an adaptive spline fitting procedure, while the parameter K^{trans} (right) is obtained from fitting a response model. The units of F_p are $[0, 0.2] \text{ min}^{-1}$ and the units of K^{trans} are $[0, 0.1] \text{ min}^{-1}$.

There are 13 data volumes in the DWI acquisition: a single T2-weighted image without diffusion weighting ($b = 0$) and 12 volumes with different gradient encodings but the same diffusion weighting. The b -value for this acquisition is $b = 1000 \text{ s/mm}^2$ (Barboriak, *personal communication*), a common value in clinical practice. As previously noted this acquisition protocol has not been optimized for ADC estimation, and will include both perfusion and diffusion effects, but is adequate for the purpose of illustration.

```
R> tensor <- system.file(file.path("nifti", sub("perfusion", "xtensor", perf)),
+                         package="dcemriS4")
R> (dwi <- readNIfTI(tensor))
R> tmask <- readANALYZE(sub(".nii", "_mask.hdr", tensor))
R> tmask <- ifelse(tmask > 0, TRUE, FALSE)
R> b <- c(0, rep(1000, ntim(dwi)-1)) # from Daniel Barboriak!
R> fit.adc <- ADC.fast(dwi, b, tmask)
R> writeNIfTI(fit.adc$S0, paste(tensor, "S0", sep="_"))
R> writeNIfTI(fit.adc$D, paste(tensor, "D", sep="_"))
```

Given the larger voxel dimensions for the DTI acquisition (5 mm slice thickness), four axial slices with a generous ROI were selected for ADC estimation and are displayed in Figure 9. The range of physical units for the ADC values is $[0.0005, 0.003] \text{ mm}^2/\text{s}$, where high ADC values correspond to the high mobility of water molecules in tissue. Thus, bright areas in the ROI may be found, for example, in the ventricles or major blood vessels and to a lesser extent the tumor(s). There appear to be areas of high diffusion in the core of each tumor when compared to either the rim of the tumor or “normal” brain tissue (white or grey matter). This

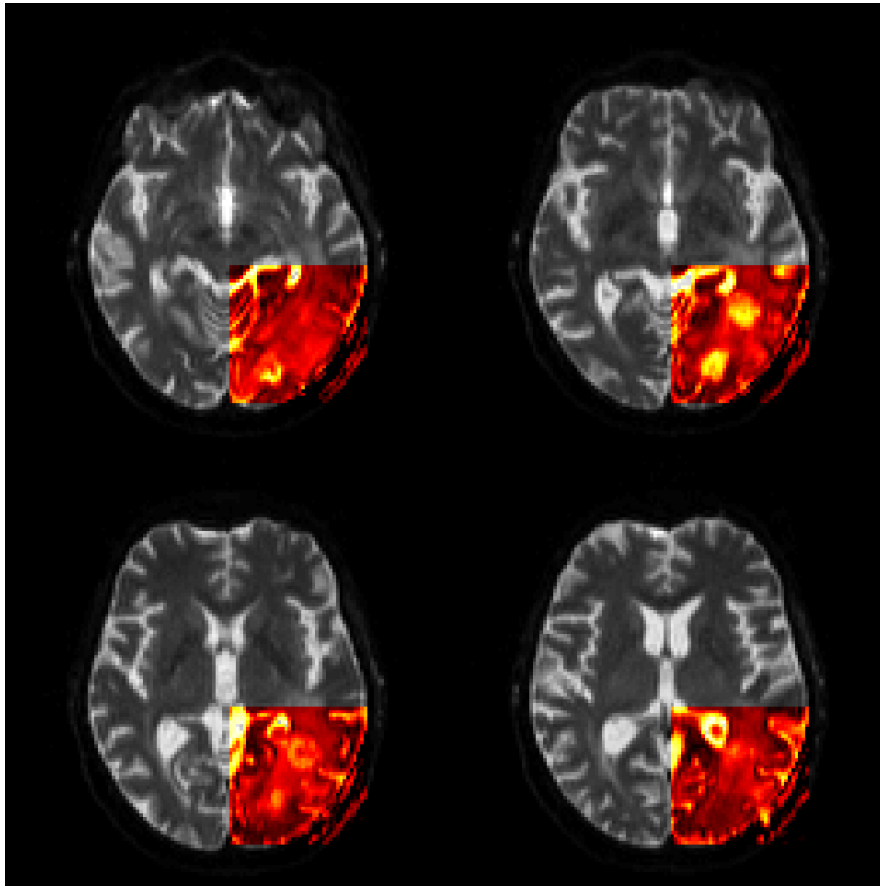


Figure 9: Statistical images of the apparent diffusion coefficient (ADC) values for the RIDER Neuro MRI data. The range of displayed values of the ADC is $[0.0005, 0.003] \text{ mm}^2/\text{s}$.

may indicate sparse cell density in the tumor “cores” due to necrotic or apoptotic processes and the subsequent removal of cells in the tissue.

The application of DWI to oncology is still a relatively immature field and caution should be used when interpreting any results because of the indirect nature of MRI data acquisition; the pharmacodynamic effects of treatment are being measured not directly in tissue, but via the diffusivity of water molecules in the tissue. However, numerous authors have published on this topic and the interested reader is encouraged to look at Koh and Padhani (2006); Yankeelov *et al.* (2007); Padhani *et al.* (2009).

Audit trail

The **dcemriS4** package supports and enhances the `audit.trail` functionality of **oro.nifti**. Hence, from any object that is stored in the `nifti` class we can trace back all the operations that have been performed on it. Figure 10 displays the XML-based audit trail for the multi-dimensional array that holds the DWI acquisition (in raw signal intensities). The main blocks of information are the `<created>`, `<saved>`, `<read>` and `<event>` tags. The first two tags occurred during the initial DICOM-to-NIfTI conversion process and the last three tags were performed during compilation of this document. In each block pertinent information has been recorded; such as the function call, version of R being used, version of the **oro.nifti** package being used, user ID, date, etc. Notice that some of these properties have changed over time, allowing one to accurately reproduce the data processing stream (if necessary).

5. Conclusions

Quantitative analysis of dynamic contrast-enhanced MRI (DCE-MRI) and diffusion-weighted imaging (DWI) data requires a series of processing steps, including pre-processing of the MR signal, voxel-wise curve fitting, and post-processing (e.g., statistical analysis of kinetic parameters from a series of scans). The **dcemriS4** package provides a comprehensive set of functions for pre-processing and parametric models for quantifying DCE-MRI and DWI data.

A (nearly) complete pipeline for the analysis of DCE-MRI and DWI data has been established in R. Acquisitions from the MR scanner, assumed to be provided in DICOM format, are converted to the NIfTI format using the **oro.dicom** and **oro.nifti** packages. Using **dcemriS4** dynamic T1-weighted acquisitions are converted into contrast agent concentration time curves on a voxel-by-voxel basis. A variety of compartmental models for the tissue kinetics, and models for the arterial input function (AIF), are available. Point estimates for kinetic parameters are provided in a fast and robust manner using either least-squares or *maximum a posteriori* techniques, and information about the uncertainty in these parameter estimates may be obtained from the Bayesian MCMC (Markov Chain Monte Carlo) algorithm; e.g., by looking at standard errors, credible intervals or the entire posterior distribution.

The **dcemriS4** package utilizes the `nifti` class defined in the **oro.nifti** package. This allows one to retain metadata information stored in the original DICOM data (e.g., patient ID or the scan date) when performing an analysis. In addition, each step in the data analysis pipeline are recorded using the audit trail capability provided by **oro.nifti**. Hence, results may be reproduced in a straightforward manner and errors in the analysis may be identified efficiently.

The **dcemriS4** package is available from CRAN (<http://CRAN.R-project.org>) and also from


```

R> audit.trail(dwi)
<audit-trail xmlns="http://www.dcemri.org/namespaces/audit-trail/1.0">
  <created>
    <call>oro.nifti::nifti(img = img, datatype = datatype)</call>
    <system>
      <r-version.version.string>R version 2.11.0 (2010-04-22)
      </r-version.version.string>
      <date>Thu May 27 08:40:18 PM 2010 BST</date>
      <user.LOGNAME>brandon</user.LOGNAME>
      <package-version.Version>0.1.4</package-version.Version>
    </system>
  </created>
  <saved>
    <workingDirectory>/home/guest/rider</workingDirectory>
    <filename>281949_19040721_axtensor</filename>
    <call>writeNIfTI(nim = uid.nifti, filename = fname)</call>
    <system>
      <r-version.version.string>R version 2.11.0 (2010-04-22)
      </r-version.version.string>
      <date>Thu May 27 08:40:23 PM 2010 BST</date>
      <user.LOGNAME>brandon</user.LOGNAME>
      <package-version.Version>0.1.4</package-version.Version>
    </system>
  </saved>
  <read>
    <workingDirectory>/home/guest/rider</workingDirectory>
    <filename>281949_19040721_axtensor.nii.gz</filename>
    <call>readNIfTI(fname = tensor)</call>
    <system>
      <r-version.version.string>R version 2.14.1 (2011-12-22)
      </r-version.version.string>
      <date>Fri Dec 30 10:01:15 2011 GMT</date>
      <user>bwhitcher</user>
      <package-version.Version>0.3.1</package-version.Version>
    </system>
  </read>
  <event>
    <type>processing</type>
    <call>ADC.fast(dwi, b, tmask)</call>
    <date>Fri Dec 30 10:01:20 2011 GMT</date>
    <user>bwhitcher</user>
  </event>
  <event>
    <type>completed</type>
    <call>ADC.fast(dwi, b, tmask)</call>
    <date>Fri Dec 30 10:01:23 2011 GMT</date>
    <user>bwhitcher</user>
  </event>
</audit-trail>

```

Figure 10: XML-based “audit trail” for the DWI acquisition of the RIDER Neuro MRI data.

SourceForge (<http://sourceforge.net/projects/dcemri>) under a BSD license. The website <http://www.dcemri.org> has been established as a convenient front end to the software development project and news items are regularly provided on the blog (<http://dcemri.blogspot.com>).

Acknowledgments

The authors would like to thank the National Biomedical Imaging Archive (NBIA), the National Cancer Institute (NCI), the National Institute of Health (NIH) and all institutions that have contributed medical imaging data to the public domain. VS is supported by the German Research Council (DFG SCHM 2747/1-1).

References

- Ahearn TS, Staff RT, Redpath TW, Semple SIK (2005). “The Use of the Levenburg-Marquardt Curve-fitting Algorithm in Pharmacokinetic Modelling of DCE-MRI Data.” *Physics in Medicine and Biology*, **50**, N85–N92.
- Bernstein MA, King KF, Zhou XJ (2004). *Handbook of MRI Pulse Sequences*. 1st edition. Elsevier, Amsterdam.
- Buckley DL (2002). “Uncertainty in the Analysis of Traced Kinetics Using Dynamic Contrast-enhanced T_1 -weighted MRI.” *Magnetic Resonance in Medicine*, **47**, 601–606.
- Buckley DL, Parker GJM (2005). “Measuring Contrast Agent Concentration in T_1 -weighted Dynamic Contrast-enhanced MRI.” In *Jackson et al. (2005)*, pp. 69–80.
- Buxton RB (2002). *Introduction to Functional Magnetic Resonance Imaging: Principles & Techniques*. Cambridge University Press, Cambridge, UK.
- Chenevert TL, Meyer CR, Moffat BA, Rehemtulla A, Mukherji SK, Gebarski SS, Quint DJ, Robertson PL, Lawrence TS, Junck L, Taylor JM, Johnson TD, Dong Q, Muraszko KM, Brunberg JA, Ross BD (2002). “Diffusion MRI: A New Strategy for Assessment of Cancer Therapeutic Efficacy.” *Molecular Imaging*, **1**(4), 336–343.
- Choyke PL, Dwyer AJ, Knopp MV (2003). “Functional Tumor Imaging with Dynamic Contrast-enhanced Magnetic Resonance Imaging.” *Journal of Magnetic Resonance Imaging*, **17**, 509–520.
- Clayden J (2011). *RNiftyReg: Medical Image Registration Using the NiftyReg Library*. R package version 0.3.1, URL <http://CRAN.R-project.org/package=RNiftyReg>.
- Collins DJ, Padhani AR (2004). “Dynamic Magnetic Resonance Imaging of Tumor Perfusion.” *IEEE Engineering in Biology and Medicine Magazine*, pp. 65–83.
- Cunningham C, Pauly J, Nayak K (2006). “Saturated Double-angle Method for Rapid B_1 + Mapping.” *Magnetic Resonance in Medicine*, **55**, 1326–1333.
- DeGroot MH (1970). *Optimal Statistical Decisions*. McGraw-Hill, New York.

- Eilers PHC, Marx BD (1996). “Flexible Smoothing with B-splines and Penalties (with Comments and Rejoinder).” *Statistical Science*, **11**(2), 89–121.
- Elzhov TV, Mullen KM, Bolker B (2010). *minpack.lm: R Interface to the Levenberg-Marquardt Nonlinear Least-Squares Algorithm Found in MINPACK*. R package version 1.1-5, URL <http://CRAN.R-project.org/package=minpack.lm>.
- Fritz-Hansen T, Rostrup E, Larsson HBW, S ndergaard L, Ring P, Henriksen O (1996). “Measurement of the Arterial Concentration of Gd-DTPA using MRI: A Step Toward Quantitative Perfusion Imaging.” *Magnetic Resonance in Medicine*, **36**, 225–231.
- Gilks WR, Richardson S, Spiegelhalter DJ (eds.) (1996). *Markov Chain Monte Carlo in Practice*. Chapman & Hall, London.
- Horsfield MA, Jones DK (2002). “Applications of Diffusion-weighted and Diffusion Tensor MRI to White Matter Diseases – A Review.” *NMR in Biomedicine*, **15**(7–8), 570–577.
- Jackson A, Buckley DL, Parker GJM (eds.) (2005). *Dynamic Contrast-Enhanced Magnetic Resonance Imaging in Oncology*. Springer, Berlin.
- Kety S (1960). “Blood–tissue Exchange Methods. Theory of Blood-tissue Exchange and its Application to Measurement of Blood Flow.” *Methods in Medical Research*, **8**, 223–227.
- Koh DM, Padhani AR (2006). “Diffusion-weighted MRI: A New Functional Clinical Technique for Tumour Imaging.” *The British Journal of Radiology*, **79**, 633–635.
- Larsson HB, Tofts PS (1992). “Measurement of the Blood-brain Barrier Permeability and Leakage Space Using Dynamic Gd-DTPA Scanning—A Comparison of Methods.” *Magnetic Resonance in Medicine*, **24**(1), 174–176.
- Larsson HBW, Stubgaard M, Frederiksen JL, Jensen M, Henriksen O, Paulson OB (1990). “Quantitation of Blood-brain Barrier Defect by Magnetic Resonance Imaging and Gadolinium-DTPA in Patients with Multiple Sclerosis and Brain Tumors.” *Magnetic Resonance in Medicine*, **16**, 117–131.
- Le Bihan D, Delannoy DJ, Levin RL (1988). “Temperature Mapping with MR Imaging of Molecular Diffusion: Application to Hyperthermia.” *Radiology*, **171**, 853–857.
- Lewis JP (1995). “Fast Template Matching.” In *Vision Interface 95, Canadian Image Processing and Pattern Recognition Society*, pp. 120–123. Quebec City, Canada. URL http://scribblethink.org/Work/nvisionInterface/vi95_lewis.pdf.
- Li KL, Zhu XP, Waterton J, Jackson A (2000). “Improved 3D Quantitative Mapping of Blood Volume and Endothelial Permeability in Brain Tumors.” *Journal of Magnetic Resonance Imaging*, **12**, 347–357.
- Marchini JL, Lafaye de Micheaux P (2009). *AnalyzefMRI: Functions for Analysis of fMRI Datasets Stored in the ANALYZE or NIFTI Format*. R package version 1.1-11, URL <http://CRAN.R-project.org/package=AnalyzefMRI>.
- Marx BD, Eilers PHC (1998). “Direct Generalized Additive Modeling with Penalized Likelihood.” *Computational Statistics & Data Analysis*, **28**(2), 193–209.

- Moré JJ (1978). “The Levenberg-Marquardt Algorithm: Implementation and Theory.” In GA Watson (ed.), *Numerical Analysis: Proceedings of the Biennial Conference held at Dundee, June 28-July 1, 1977*, Lecture Notes in Mathematics #630, pp. 104–116. Springer-Verlag, Berlin.
- Moseley ME, Cohen Y, Kucharczyk J, Mintorovitch J, Asgari HS, Wendland MF, Tsuruda J, Norman D (1990). “Diffusion-weighted MR Imaging of Anisotropic Water Diffusion in Cat Central Nervous System.” *Radiology*, **176**(2), 439–445.
- O’Connor E, Fieller N, Holmes A, Waterton JC, Ainscow E (2010). “Functional Principal Component Analyses of Biomedical Images as Outcome Measures.” *Journal of the Royal Statistical Society C (Applied Statistics)*, **59**(1), 57–76.
- Orton MR, d’Arcy JA, Walker-Samuel S, Hawkes DJ, Atkinson D, Collins DJ, Leach MO (2008). “Computationally Efficient Vascular Input Function Models for Quantitative Kinetic Modelling Using DCE-MRI.” *Physics in Medicine and Biology*, **53**, 1225–1239.
- Padhani A, Liu G, Koh DM, Chenevert TL, Thoeny HC, Takahara T, Dzik-Jurasz A, Ross BD, Van Cauteren M, Collins D, Hammoud DA, Rustin GJS, Taouli B, Choyke PL (2009). “Diffusion Weighted Magnetic Resonance Imaging (DW-MRI) as a Cancer Biomarker: Consensus Recommendations.” *Neoplasia*, **11**(2), 102–125.
- Parker GJM, Padhani AR (2003). “ T_1 -w DCE-MRI: T_1 -weighted Dynamic Contrast-enhanced MRI.” In *Tofts* (2003), chapter 10, pp. 341–364.
- Parker GJM, Roberts C, Macdonald A, Buonaccorsi GA, Cheung S, Buckley DL, Jackson A, Watson Y, Davies K, Jayson GC (2006). “Experimentally-derived Functional Form for a Population-averaged High-temporal-resolution Arterial Input Function for Dynamic Contrast-enhanced MRI.” *Magnetic Resonance in Medicine*, **56**, 993–1000.
- R Development Core Team (2011). *R: A Language and Environment for Statistical Computing*. R Foundation for Statistical Computing, Vienna, Austria. ISBN 3-900051-07-0, URL <http://www.R-project.org>.
- Schmid V, Whitcher B, Padhani AR, Taylor NJ, Yang GZ (2006). “Bayesian Methods for Pharmacokinetic Models in Dynamic Contrast-enhanced Magnetic Resonance Imaging.” *IEEE Transactions on Medical Imaging*, **25**(12), 1627–1636.
- Schmid VJ, Whitcher B, Padhani AR, Taylor NJ, Yang GZ (2009a). “A Bayesian Hierarchical Model for the Analysis of a Longitudinal Dynamic Contrast-enhanced MRI Oncology Study.” *Magnetic Resonance in Medicine*, **61**(1), 163–174.
- Schmid VJ, Whitcher B, Padhani AR, Yang GZ (2009b). “Quantitative Analysis of Dynamic Contrast-enhanced MR Images Based on Bayesian P-splines.” *IEEE Transactions on Medical Imaging*, **28**(6), 789–798.
- St Lawrence KS, Lee TY (1998). “An Adiabatic Approximation to the Tissue Homogeneity Model for Water Exchange in the Brain: I. Theoretical Derivation.” *Journal of Cerebral Blood Flow and Metabolism*, **18**(12), 1365–77.

- Tabelow K, Clayden JD, Lafaye de Micheaux P, Polzehl J, Schmid VJ, Whitcher B (2011). “Image Analysis and Statistical Inference in Neuroimaging with R.” *NeuroImage*, **55**(4), 1686–1693.
- Tofts P (ed.) (2003). *Quantitative MRI of the Brain: Measuring Changes Caused by Disease*. Wiley, Chichester, UK.
- Tofts PS, Kermode AG (1984). “Measurement of the Blood-brain Barrier Permeability and Leakage Space using Dynamic MR Imaging. 1. Fundamental Concepts.” *Magnetic Resonance in Medicine*, **17**(2), 357–367.
- Wang HZ, Riederer SJ, Lee JN (1987). “Optimizing the Precision in T1 Relaxation Estimation Using Limited Flip Angles.” *Magnetic Resonance in Medicine*, **5**, 399–416.
- Weinmann HJ, Laniado M, Mutzel W (1984). “Pharmacokinetics of Gd-DTPA/dimeglumine After Intravenous Injection into Healthy Volunteers.” *Physiological Chemistry and Physics and Medical NMR*, **16**, 167–172.
- Wheeler-Kingshott CAM, Barker GJ, Steens SCA, van Buchem MA (2003). “D: the Diffusion of Water.” In [Tofts \(2003\)](#), chapter 7, pp. 203–256.
- Whitcher B, Schmid V, Thornton A (2011). *oro.nifti: Rigorous - NIfTI Input / Output*. R package version 0.2.6, URL <http://CRAN.R-project.org/package=oro.nifti>.
- Whitcher B, Schmid VJ (2011). “Quantitative Analysis of Dynamic Contrast-Enhanced and Diffusion-Weighted Magnetic Resonance Imaging for Oncology in R.” *Journal of Statistical Software*, **44**(5), 1–29. URL <http://www.jstatsoft.org/v44/i05/>.
- Yankeelov TE, Lepage M, Chakravarthy A, Broome EE, Niernann KJ, Kelley MC, Meszoely I, Mayer IA, Herman CR, McManus K, Price RR, Gore JC (2007). “Integration of Quantitative DCE-MRI and ADC Mapping to Monitor Treatment Response in Human Breast Cancer: Initial Results.” *Magnetic Resonance Imaging*, **25**, 1–13.

Affiliation:

Brandon Whitcher
 Mango Solutions
 Office 202, Second Floor
 14 Greville Street
 London EC1N 8SB, United Kingdom
 E-mail: bwhitcher@mango-solutions.com
 URL: <http://www2.imperial.ac.uk/~bwhitcher>, <http://www.dcemri.org>

Volker J. Schmid
 Bioimaging group
 Department of Statistics
 Ludwig-Maximilians Universität München, Germany
 E-mail: volker.schmid@lmu.de
 URL: <http://volkerschmid.de>